Towards Implementation of Advanced Bioheat Models in Human Head Exposed to 5G Radiation

Ivan Dominik Horvat
Faculty of Mechanical Engineering
University of Maribor
Maribor, Slovenia
ivan.horvat@um.si

Jana Wedel
Lehrstuhl für Technische Mechanik
Friedrich-Alexander-Universität
Erlangen, Germany
jana.wedel@fau.de

Nejc Vovk
Faculty of Mechanical Engineering
University of Maribor
Maribor, Slovenia
nejc.vovk@um.si

Blaž Kamenik
Faculty of Mechanical Engineering
University of Maribor
Maribor, Slovenia
blaz.kamenik@um.si

Paul Steinmann
Lehrstuhl für Technische Mechanik
Friedrich-Alexander-Universität
Erlangen, Germany
paul.steinmann@fau.de

Jure Ravnik
Faculty of Mechanical Engineering
University of Maribor
Maribor, Slovenia
jure.ravnik@um.si

***Abstract*—This study presents the implementation and validation of the Pennes bioheat equation within the OpenFOAM framework to simulate heat transfer in human head tissues, with the aim to be able to model the human head exposed to 5G millimeter wave radiation. We implement a bioheat solver based and validate it through benchmark problems, including a cylindrical tissue domain with an analytical solution and a multi-layer tissue configuration. In addition, we simulate heat transfer in a high-resolution human head model incorporating heterogeneous tissue properties from the IT'IS database. Results confirm the solver's accuracy and stability, and temperature predictions align with experimental data from the literature. This work lays the foundation for advanced electromagnetic-thermal dosimetry modeling in realistic anatomical geometries, contributing to the ongoing assessment of 5G-related health effects.**

***Index Terms*—Bioheat, Pennes equation, OpenFOAM, 5G radiation, human head modeling, SAR, mmWave.**

I. Introduction

The bioheat equation modeling in the context of the human head's exposure to 5G radiation has emerged as a crucial field of study due to the increasing adoption of millimeter wave (mmWave) technology. This modeling is essential for understanding the thermal responses and specific absorption rate (SAR) induced by electromagnetic fields associated with 5G networks, particularly as these networks often operate at high frequencies, such as 28 GHz. The bioheat equation, grounded in Pennes' heat transfer model, is integral to evaluating the thermal effects resulting from electromagnetic exposure.

Cvetković et al. [2] show this by coupling electromagnetic (EM) dosimetry with thermal dosimetry, demonstrating that EM fields can induce temperature changes in biological tissues when modeled through finite element methods (FEM). Their work highlights that the induced heating in tissues, particularly in the human head, significantly depends on the electric field distribution generated by mmWave frequencies. This is corroborated by Hamed and Maqsood [7], who explored the SAR and temperature rise across various mmWave frequencies, utilizing finite difference time domain (FDTD) simulations to assess the thermal implications of EM exposure.

Furthermore, the practical implications of exposure to 5G are illustrated by Morelli et al. [12], who conducted numerical analyses to simulate the SAR profiles during mobile communication, emphasizing the variations in exposure levels between adults and children. The results suggested that the biological response, including temperature elevation due to absorbed power, differs significantly based on the age and anatomical models employed. This aligns with the findings from Penta and Kumar [15], who specifically targeted SAR reduction techniques pertinent to the head area under 5G influence, evidencing concerns over temperature fluctuations due to high SAR in mobile communication scenarios. The biological implications of 5G radiation extend beyond mere thermal considerations.

Hardell and Nyberg [8] raised critical concerns regarding the lack of comprehensive scientific evaluations prior to the deployment of 5G technologies, linking RF exposure to various health risks including cognitive and neurobehavioral impacts.

In contrast, the review by Karipidis et al. [11] states that although numerous studies have been carried out in low-level RF fields, there remains minimal evidence of health effects associated with the frequencies used in 5G technologies, calling for improved research methodologies. This reflects the ongoing debate about the safety of prolonged exposure to high-frequency EM fields. In addition to health risks, the modeling frameworks must also consider the increasing complexity of exposure conditions with the deployment of 5G infrastructure.

Elbasheir et al. [5] demonstrated through exposure assess-

The authors would like to acknowledge the support of ARIS (J7-60118) and HRZZ (IPS-2024-02-7779) in the framework of the project: HER-WICT - Human Exposure to Radiation from new Wireless Communication Technologies using Advanced Electromagnetic-Thermal Dosimetry Models. Furhtermore, the authors would like to acknowledge the support of Deutsche Forschungsgemeinschaft (STE 544/75-1).

ments that exposure levels are contingent upon urban density and specific base station configurations, further complicating the modeling scenarios. This is essential since varying environmental conditions can influence SAR and temperature responses in biological tissues. In conclusion, the integration of bioheat equation modeling in the assessment of human head exposure to 5G radiation is pivotal in understanding both thermal responses and broader health implications. Emerging evidence necessitates further research efforts focusing on redefining models to encapsulate the complexities of human exposure to new-generation wireless communication technologies.

In this paper, we describe the implementation and validation of the Pennes bioheat equation in the OpenFOAM framework for simulating heat transfer in human head tissues, with the goal of modeling the head exposed to 5G millimeter wave radiation under different air flow regime. The bioheat solver is validated using benchmark problems, including a cylindrical tissue domain with an analytical solution and a multi-layer tissue configuration. Furthermore, we simulate heat transfer in a human head model consisting of 11 distinct tissue types.

II. Governing Equation

The Pennes [14] bioheat equation

$$\rho c_t \frac{\partial T}{\partial t} = \nabla \cdot [k \nabla T] + w_b c_b [T_a - T] + Q_m, \qquad (1)$$

is a widely used model for heat transfer in biological tissues. The equation describes the temperature field T in a tissue with density ρ, specific heat c_t, thermal conductivity k, and metabolic heat generation Q_m. The properties are tissue specific and assumed constant within tissues. Here w_b $[kg/(m^3 s)]$ is the blood perfusion rate per unit volume, c_b is the specific heat of blood, and T_a is the temperature of arterial blood. The equation is typically solved in a domain Ω with boundary $\partial\Omega$ and initial condition. The boundary conditions are typically of the Robin type, with a heat transfer coefficient h and a temperature T_∞.

III. Implementation

We implement the governing equation (1) into OpenFOAM [20] and test the validity of the implementation by considering a tissue with constant material properties and steady state conditions. OpenFOAM (Open Field Operation and Manipulation) is an open-source CFD toolbox designed for the development of customized numerical solvers and pre-/post-processing utilities for the solution of continuum mechanics problems, primarily fluid flow governed by the Navier-Stokes equations. Written in C++ and leveraging object-oriented principles, OpenFOAM provides a flexible and extensible platform for high-fidelity simulations across a wide range of applications, from incompressible and compressible flows to multiphase, turbulent, and reactive systems. Its architecture is built around a modular class structure that abstracts complex operations such as discretization, linear algebra, and parallelization (via MPI), enabling advanced users to tailor solvers and boundary conditions with minimal overhead. OpenFOAM considers total energy from of the Pennes equation, $e = c_t[T - T_{\text{ref}}] + \frac{1}{2}v^2 + gz$, where c_t is the specific heat, T_{ref} is the reference temperature, v is the magnitude of the velocity vector and g is the gravitational acceleration. For constant material properties, the Pennes equation can be written in the form

$$\rho \frac{\partial e}{\partial t} = \nabla \cdot \left[\frac{k}{c} \nabla e\right] + c_b \omega_b \left[T_a - \frac{e}{c} - T_{\text{ref}}\right] + Q_m \qquad (2)$$

where kinetic and potential energy contributions were neglected.

IV. Benchmarking

To verify the implementation of the Pennes equation in OpenFOAM, we consider two test cases. The first test case is a radially symmetric cylinder with constant material properties, where the analytical solution is available. The second considers different tissues and verifies energy conservation across boundaries.

A. Pennes equation in a cylinder

To benchmark the implementation we consider a cylinder with radius R and length L, where $L \gg R$. The equation can then be solved in the radial direction only, with the assumption of axial symmetry. When the following boundary conditions are chosen:

$$\frac{dT}{dr} = 0, \qquad r = 0, \qquad (3)$$

$$-k\frac{dT}{dr} = h[T - T_\infty], \qquad r = R, \qquad (4)$$

an analytical solution of the problem exists, which can be used to validate the numerical implementation.

1) Analytical solution: In the benchmark case the temperature depends on radial direction only and thus the Laplace operator simplifies to $\frac{1}{r}\frac{d}{dr}\left[r\frac{dT}{dr}\right]$. The Pennes equation, written for temperature, then reads

$$\frac{1}{r}\frac{d}{dr}\left[r\frac{dT}{dr}\right] + \frac{w_b c_b}{k}[T_a - T] + \frac{Q_m}{k} = 0. \qquad (5)$$

The analytical solution for the Pennes equation in a cylinder was derived by [21]. They used the following nondimensional variables:

$$r^* = \frac{r}{R}, \quad T^* = \frac{T - T_\infty}{T_a - T_\infty}, \quad \theta = \frac{w_b c_b R^2}{k},$$
$$\gamma = \frac{Q_m R^2}{k[T_a - T_\infty]}, \quad \alpha = \frac{hR}{k}. \qquad (6)$$

The nondimensional Pennes equation then reads

$$\frac{1}{r^*}\frac{d}{dr^*}\left[r^*\frac{dT^*}{dr^*}\right] + \theta[1 - T^*] + \gamma = 0. \qquad (7)$$

The nondimensional boundary conditions are

$$\frac{dT^*}{dr^*} = 0, \qquad r^* = 0, \qquad (8)$$

$$\frac{dT^*}{dr^*} = -\alpha T^*, \qquad r^* = 1. \qquad (9)$$

The analytical solution for the nondimensional temperature field is

$$T^*(r^*) = \left[1 + \frac{\gamma}{\theta}\right]\left[1 - \frac{I_0\left[r^*\sqrt{\theta}\right]}{I_0\left[\sqrt{\theta}\right] + \frac{\sqrt{\theta}}{\alpha} I_1\left[\sqrt{\theta}\right]}\right], \quad (10)$$

where I_0 and I_1 are modified Bessel functions of the first kind.

2) Numerical solution: The test case is a cylinder with radius $R = 0.045$ m. The tissue material properties are $c_b = 3850$ J/(kg K), $k = 0.48$ W/(m K), $w_b = 3$ kg/(m^{3}s), $T_a = 310$ K, $Q_m = 1085$ W/m^3, $h = 10.023$ W/(m^2 K), $T_\infty = 298$ K. The nondimensional parameters are $\theta = 97.45$, $\gamma = 0.7629$, $\alpha = 1.879$.

Comparison between the analytical solution (10) and our simulations is shown in Figs. 1, 2, and 3 where temperature distribution versus the radial position is shown for several values of thermal conductivity, blood perfusion rate per unit volume and metabolic heat generation, respectively. We observe excellent agreement for all computational grids used.

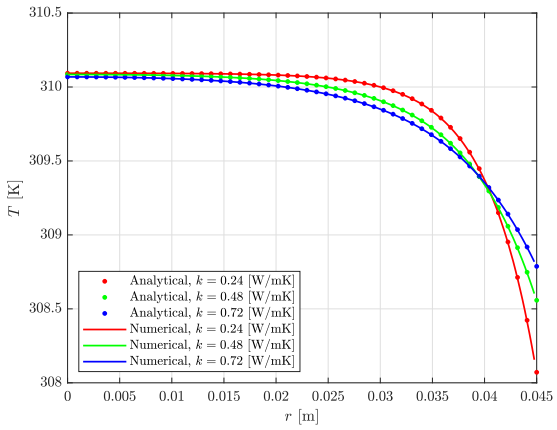

Fig. 1. Comparison of tissue temperature simulation results and analytical evaluation of (10) for temperature versus radial position for various values of thermal conductivity.

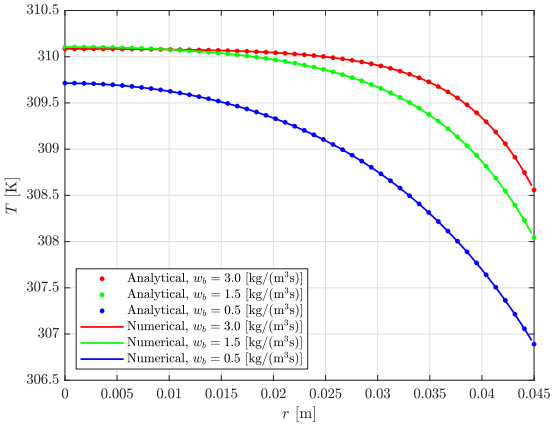

Fig. 2. Comparison of tissue temperature simulation results and analytical evaluation of (10) for temperature versus radial position for various values of blood perfusion rate per unit volume.

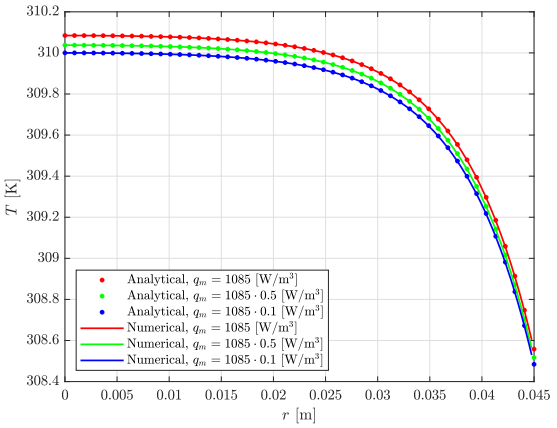

Fig. 3. Comparison of tissue temperature simulation results and analytical evaluation of (10) for temperature versus radial position for various values of metabolic heat generation.

B. Multiple tissues test case

To verify the ability of the numerical algorithm to handle multiple tissues we consider a 1D temperature distribution problem within three joined subdomains, adapted from [16]. The domain is a long cylinder of diameter 1 m and length 3 m made of three different materials, as shown in Figure 4. The prescribed potential is at the top and bottom of the cylinder is $T_0 = 1°C$, $T_3 = 4°C$ and the conductivities are $k_1 = 4\ W/mK$, $k_2 = 3\ W/mK$, $k_3 = 2\ W/mK$. There is no heat flux at the cylinder wall, so the problem is one-dimensional. The analytical solution for the temperature between the subdomains is $T_1 = 22/13 = 1.6923°C$, $T_2 = 34/13 = 2.6154°C$ and for the heat flux is $q = 36/13 = 2.7692\ W/m^2$. The results are shown in Fig. 5. They show that the numerical solution matches the analytical solution very closely for both temperature and heat flux.

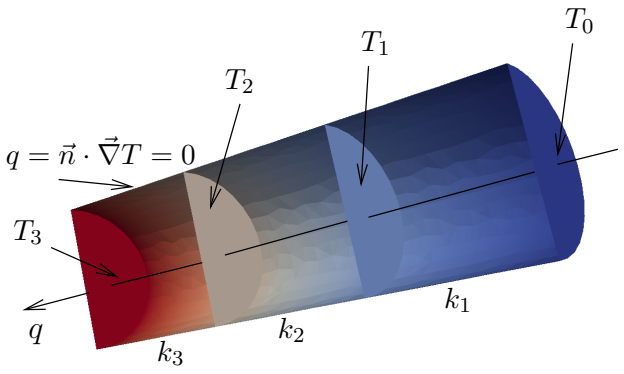

Fig. 4. Temperature distribution in the case of one-dimensional heat diffusion problem with three subdomains. Constant temperature T_0 and T_3 are prescribed at the top and bottom ends of the cylinder, whereas zero flux is assumed at the cylinder surface.

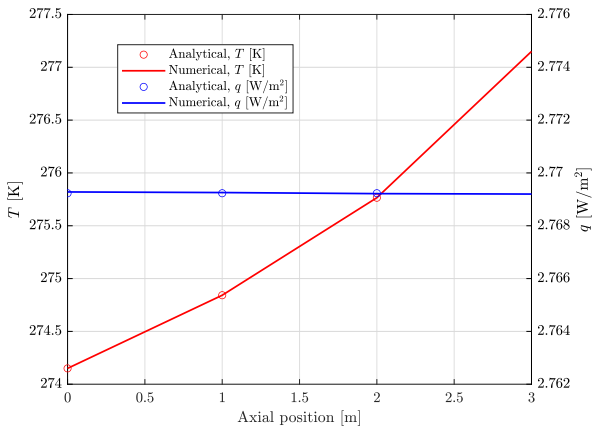

Fig. 5. Comparison of the numerical solution with the analytical solution for the temperature and heat flux in the three subdomains.

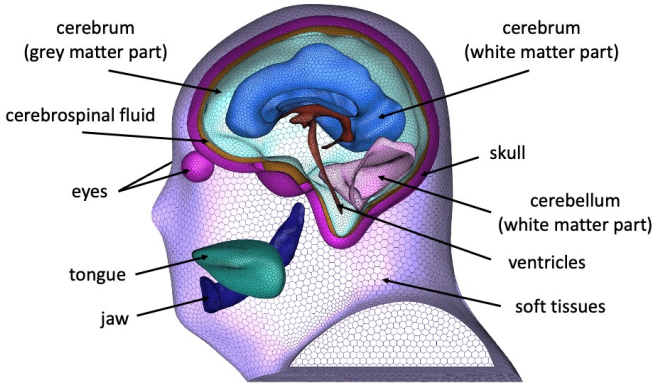

Fig. 6. The Eleven subdomain head model, [6], [13].

V. Human head model

A. Setup

The human head is a complex structure composed of various tissues, each with distinct thermal properties and biological activity. Understanding the heat transfer phenomena in the human head is crucial for evaluating the effects of electromagnetic radiation on biological tissues, particularly in the context of 5G millimeter wave exposure. In this section we present the use of the Pennes bioheat equation, which we implemented in OpenFOAM, to model the heat transfer in the human head validate it against existing literature.

Rzechorzek et al. [17] found that in healthy people, brain temperature ranged from 36.1°C to 40.9°C, with a mean of 38.5 ± 0.4°C, exceeding oral temperature (36.0 ± 0.5°C). Tan et al. [18] demonstrated that brain temperature (38.51 ± 0.59°C) is significantly higher than body temperature (36.47 ± 0.26°C), confirming a brain-body temperature gradient. The scalp skin temperature was shown to be in the range of 34.4 °C (Janssen et al. [10]). Daanen et al. [3] reported the scalp temperature to be 32.1 ± 0.5 °C, the forehead temperature 33.9 ± 0.4 °C and the skin temperature of 32.3 ± 0.4 °C with the core body (esophageal) temperature 36.5 ± 0.2°C.

We employ the human head model of Noetscher, et al. [6], [13]. The model is shown in Fig. 6. The subdomains included in the model are the cerebrum (grey and white matter), cerebellum (white matter), skull, jaw, tongue, eye, soft tissues, blood and cerebrospinal fluid (CSF). We assume that the skull and jaw are made of 65% cortical, 35% cancellous bone.

To facilitate the use of the finite volume method, which is implemented in OpenFOAM, to discretize the bioheat transfer equation, the human head model is discretized per subdomain basis. We prepared three meshes with 881k elements (coarse), 2.11 mio elements (medium) and 10.04 mio elements (fine). The meshes are shown in Fig. 7.

We obtained the tissue properties from the IT'IS database [9]. We assume [19] that the arterial blood temperature is equal to the core body temperature, which is $T_a = 37$ °C. The tissue properties are summarized in Table I.

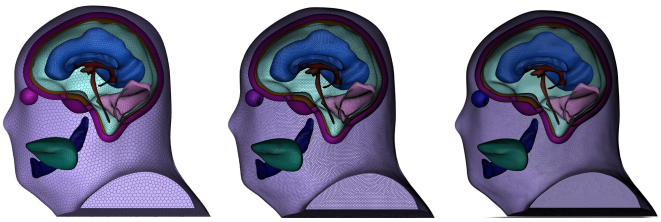

Fig. 7. The three meshes used to simulate bioheat transport in the head model, coarse mesh (881k elements, left), medium (2.11 mio, center) and fine (10.04 mio, right)

B. Boundary conditions

For a human standing in still air, heat is lost primarily through radiation and convection. Experimental [4] and numerical [1] studies measured and estimated the convective and radiative heat transfer coefficients for the human head in still air. The convective heat transfer coefficient was found to be 3.6 W/(m^{2}K) and the linear radiative heat transfer coefficient was found to be 4.1 W/(m^{2}K), which makes the total heat transfer coefficient equal to $h = 7.7$ W/(m^{2}K). This was used in the Robin type boundary condition at the skin surface $q = h[T - T_\infty]$. The temperature of the environment was set to $T_\infty = 20$ °C. At the bottom of the model, where the model is cut from the lower body, we used the adiabatic boundary condition to assume no heat exchange between the head and the body.

C. Results

In our bioheat transfer model heat is transported via diffusion and perfusion. Both processes are unlikely to produce sharp temperature gradients in the human head. Nevertheless, we performed a mesh convergence study to ensure that the numerical solution is not sensitive to the mesh density. We used the fine mesh for the simulation and compared the results

TABLE I
TISSUE PROPERTIES, [9]

Tissue	ρ [kg/m^3]	c_p [J/kg·K]	k [W/m·K]	w_b [kg/m^{3}s]	Q_m [W/m^3]
Cerebrum (grey matter)	1044.5	3695.8	0.547	13.9555	16230
Cerebrum (white matter)	1041	3582.8	0.481	3.8673	4498
Cerebellum (white matter)	1045	3653	0.506	14.078	16373
Skull, Jaw	1653	1649.2	0.32	0.4915	435
Tongue	1090.4	3421.2	0.4950	1.4880	1317
Eye	1053.2	3583.0	0.5132	20.1063	22683
Soft tissues	1109	3390.5	0.3722	2.0641	1827
CSF, ventricles	1007	4095.5	0.5733	0	0
Blood	1049.75	3617	-	-	-

with the medium and coarse meshes. A profile of temperature along the z-axis is shown in Fig. 8, where the results clearly demonstrate that the temperature distribution is not sensitive to the mesh density.

The temperature distribution in the head model is shown in Figs. 9, 10 and 11. We observe that the temperature distribution is not uniform and that the temperature is higher in the brain than in the skin. This is due to the fact that the blood perfusion rate is much higher in the brain and that the cooling occurs across the skin surface. The temperature distribution is also affected by the presence of the skull, which acts as an insulator and reduces heat transfer from the brain to the skin.

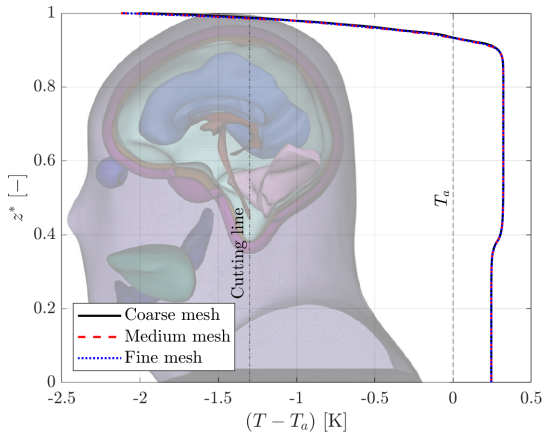

Fig. 8. Temperature profile along the z-axis, normalized to the head model height; z^*. Line definition (x, y, z): start (0.0075, 0.025, -0.115); end (0.0075, 0.025, 0.1418)

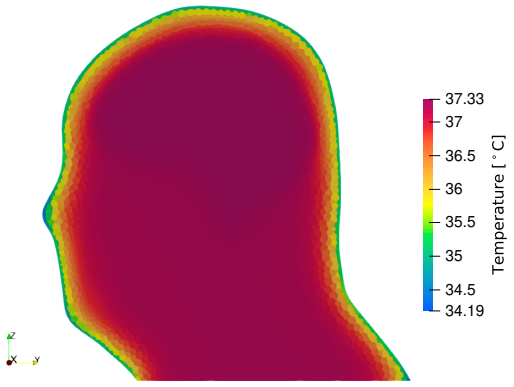

Fig. 9. Temperature distribution on a x-normal plane at $x = 0.0075$ m

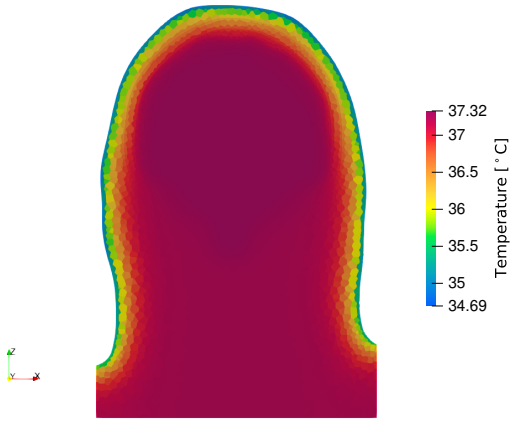

Fig. 10. Temperature distribution on a y-normal plane at $y = 0.025$ m

VI. CONCLUSION

In this work, we presented the implementation of the Pennes bioheat equation within the OpenFOAM framework to simulate heat transfer in biological tissues, with particular focus on human head exposure to 5G millimeter wave (mmWave) radiation. The bioheat solver was validated against two benchmark cases: an analytical cylindrical tissue model and a multilayer tissue configuration. Each validation confirmed the solver's numerical accuracy, robustness, and agreement with theoretical expectations.

We extended our investigation to a high-fidelity anatomical model of the human head composed of 11 heterogeneous tissue domains with physical properties derived from the IT'IS database. The simulations revealed physiologically plausible temperature distributions that aligned with empirical literature, notably showing elevated core brain temperatures and a gradient toward cooler skin layers due to blood perfusion and surface heat loss.

The successful implementation and validation of this model lays the foundation for the future integration of electromagnetic exposure data to perform comprehensive

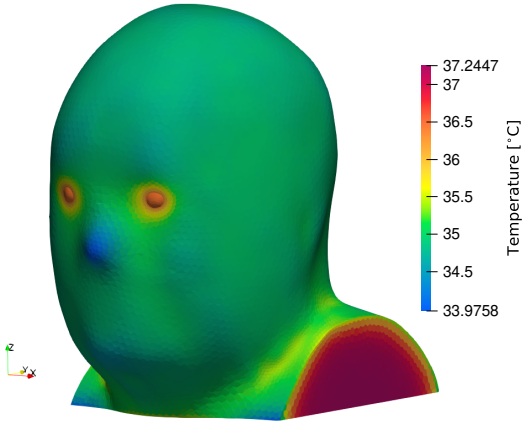

Fig. 11. Temperature distribution on the head model surface.

electromagnetic-thermal dosimetry. This is particularly important in view of the growing public interest in health and the scientific investigation of the potential biological effects of 5G radiation. By providing an open-source, extensible numerical framework, this research contributes a crucial step towards more realistic and anatomically sound assessments of human exposure to next-generation wireless communication technologies.

Future work will focus on coupling this thermal model with full-wave electromagnetic solvers to simulate SAR distribution under realistic exposure scenarios and extend the scope to include age-dependent anatomical variations and transient exposure effects.

REFERENCES

[1] Zubieda Alali and S.J. Eckels. 3D numerical simulations of mixed convective heat transfer and correlation development for a thermal manikin head. *Heliyon*, 10(9):e30161, May 2024.

[2] Mario Cvetkovic, Hrvoje Dodig, and Dragan Poljak. On some computational aspects for electromagnetic-thermal dosimetry of mm waves. *Journal of Physics: Conference Series*, 2766(1):012193, May 2024.

[3] Hein A. M. Daanen, Mijke Peerbooms, Corina J. G. Van Den Hurk, Bernadet Van Os, Koen Levels, Lennart P. J. Teunissen, and Wim P. M. Breed. Core temperature affects scalp skin temperature during scalp cooling. *International Journal of Dermatology*, 54(8):916–921, August 2015.

[4] R. J. De Dear, Edward Arens, Zhang Hui, and Masayuki Oguro. Convective and radiative heat transfer coefficients for individual human body segments. *International Journal of Biometeorology*, 40(3):141–156, May 1997.

[5] Mohammed S. Elbasheir, Rashid A. Saeed, and Salaheldin Edam. Measurement and Simulation-Based Exposure Assessment at a Far-Field for a Multitechnology Cellular Site up to 5G NR. *IEEE Access*, 10:56888–56900, 2022.

[6] Jeffrey M. Elloian, Gregory M. Noetscher, Sergey N. Makarov, and Alvaro Pascual-Leone. Continuous Wave Simulations on the Propagation of Electromagnetic Fields Through the Human Head. *IEEE Transactions on Biomedical Engineering*, 61(6):1676–1683, June 2014.

[7] Tooba Hamed and Moazam Maqsood. Sar Calculation & Temperature Response Of Human Body Exposure To Electromagnetic Radiations At 28, 40 And 60 Ghz Mmwave Frequencies. *Progress In Electromagnetics Research M*, 73:47–59, 2018.

[8] Lennart Hardell and Rainer Nyberg. Appeals that matter or not on a moratorium on the deployment of the fifth generation, 5G, for microwave radiation. *Molecular and Clinical Oncology*, January 2020.

[9] IT'IS Foundation. Tissue Properties Database V4.2, 2024.

[10] F E M Janssen, G M J Van Leeuwen, and A A Van Steenhoven. Modelling of temperature and perfusion during scalp cooling. *Physics in Medicine and Biology*, 50(17):4065–4073, September 2005.

[11] Ken Karipidis, Rohan Mate, David Urban, Rick Tinker, and Andrew Wood. 5G mobile networks and health—a state-of-the-science review of the research into low-level RF fields above 6 GHz. *Journal of Exposure Science & Environmental Epidemiology*, 31(4):585–605, July 2021.

[12] Maria Sole Morelli, Silvia Gallucci, Beatrice Siervo, and Valentina Hartwig. Numerical Analysis of Electromagnetic Field Exposure from 5G Mobile Communications at 28 GHZ in Adults and Children Users for Real-World Exposure Scenarios. *International Journal of Environmental Research and Public Health*, 18(3):1073, January 2021.

[13] Gregory M. Noetscher, Janakinadh Yanamadala, Sergey N. Makarov, and Alvaro Pascual-Leone. Comparison of Cephalic and Extracephalic Montages for Transcranial Direct Current Stimulation—A Numerical Study. *IEEE Transactions on Biomedical Engineering*, 61(9):2488–2498, September 2014.

[14] Harry H. Pennes. Analysis of Tissue and Arterial Blood Temperatures in the Resting Human Forearm. *Journal of Applied Physiology*, 1(2):93–122, August 1948.

[15] Ashok Kumar Penta and Ch. R. Phani Kumar. A Novel PIFA Design for SAR Reduction in 5G Networks to Analyze the RF Shield *I*mpact. *Engineering, Technology & Applied Science Research*, 14(3):14102–14108, June 2024.

[16] Jure Ravnik, Anna Šušnjara, Ožbej Verhnjak, Dragan Poljak, and Mario Cvetković. Coupled Boundary Element Method: A Stochastic Collocation Approach for Uncertainty Estimation in Transcranial Electric Stimulation Simulations. In *Boundary Elements and Other Mesh Reduction Methods XLIV*, pages 145–155, August 2021.

[17] Nina M Rzechorzek, Michael J Thrippleton, Francesca M Chappell, Grant Mair, Ari Ercole, Manuel Cabeleira, The CENTER-TBI High Resolution ICU (HR ICU) Sub-Study Participants and Investigators, Jonathan Rhodes, Ian Marshall, and John S O'Neill. A daily temperature rhythm in the human brain predicts survival after brain injury. *Brain*, 145(6):2031–2048, June 2022.

[18] Yahong Tan, Wenjia Liu, Yanhua Li, Nan Zhang, Mingxiao Wang, Shuo Sun, and Lin Ma. Measurement of Healthy Adult Brain Temperature Using 1H Magnetic Resonance Spectroscopy Thermometry. *Clinical Neuroradiology*, 35(1):159–164, March 2025.

[19] Jonathan W. Valvano. Bioheat Transfer. In John G. Webster, editor, *Encyclopedia of Medical Devices and Instrumentation*. Wiley, 1 edition, April 2006.

[20] H G Weller, G Tabor, H Jasak, and C Fureby. A tensorial approach to computational continuum mechanics using object-oriented techniques. *Computers in Physics*, 12(6):620–631, 1998.

[21] Kai Yue, Xinxin Zhang, and Fan Yu. An analytic solution of one-dimensional steady-state Pennes' bioheat transfer equation in cylindrical coordinates. *Journal of Thermal Science*, 13(3):255–258, August 2004.